Contents lists available at SciVerse ScienceDirect

CIRP Annals Manufacturing Technology

Journal homepage: www.elsevier.com/locate/cirp

# Manipulating Martensite Transformation of SS304L During Double-Sided Incremental Forming by Varying Temperature and Deformation Path

Shayan Darzi, Matt D. Adams, John T. Roth, Brad L. Kinsey (2), Jinjin Ha

*Department of Mechanical Engineering, University of New Hampshire, Durham, NH 03824, USA*

Double-sided incremental forming (DSIF) is a die-less sheet metal forming process capable of fabricating complex parts. The flexibility of DSIF can be used for in-situ mechanical properties alteration, e.g., by controlling deformation-induced martensite transformation of austenitic stainless steels. In this paper, SS304L is deformed using DSIF at three different cooling conditions and two different tool paths to affect the martensite transformation. Additionally, finite element analyses were used to understand the effect of tool paths on springback and plastic strain. Implementing a reforming tool path at the lowest achievable temperature resulted in a martensite volume fraction as high as 95%.

Incremental sheet forming, Finite element method, Strain-induced martensite transformation

## 1. Introduction

In the last 20 years, incremental forming (IF) has been successfully introduced as a rapid, flexible prototyping process for concept parts or small-batch production of sheet metal components. One, two, or more tools following prescribed paths deform the workpiece locally [1], and their variations determine the process [2], such as single point (SPIF) and double-sided IF (DSIF). Major advantage of IF over other processes is greater forming flexibility, which is inherent from die-less feature creation. It allows customization of parts and significantly reduces lead-times and tooling costs.

IF benefits from superior formability compared to conventional forming processes [2]. For example, Moser et al. [3] was able to improve formability of the process by use of a reforming operation. On the contrary, geometrical accuracy has always been a concern for the industrial use of IF. Wang et al. [4] found that springback of the trimmed cone part can be reduced using a higher squeeze factor during DSIF as well as overbending exerted by the support tool during forming. The squeeze factor is defined as a coefficient (less than 1) multiplied by the thickness of the sheet calculated by sine law, which determines the amount of "squeezing" of the sheet at the location between the two tools.

In addition to experimental studies, numerical simulations have been applied to understand the IF process. A modified Gurson-Tvergaard-Needleman (GTN) damage model was developed by Peng and Ou [5], capable of accurately predicting the fracture depth for SPIF and DSIF. They found that the additional compression caused by the support tool in DSIF leads to a reduction in stress triaxiality and through-thickness shear and therefore higher formability. Other researchers have used numerical simulations to improve the accuracy of the IF process. Ren et al. [6] were able to reduce the springback by use of an offline simulation-based model with an in-situ compensation loop for the tool path. In another study, Moser et al. [7] incorporated machine compliance into their DSIF model and were able to predict geometries, strains, and forces with better accuracy than rigid tool models.

Forming flexibility of IF can allow manipulating mechanical properties of formed parts through microstructure control. For example, an austenitic stainless steel with deformation-induced martensite transformation can produce varied mechanical properties depending on the process conditions, e.g., deformation path, stress state, strain rate, and temperature [8–10]. As a result, locally heterogeneous properties can be achieved by controlling the martensite transformation kinetics during deformation. For example, a cranial trauma fixation implant fabricated with location-specific loading paths can increase strength around the screw locations, while maintaining ductility in other areas.

In this study, the effect of temperature and deformation path on the deformation-induced martensite transformation during DSIF of an austenitic stainless steel (SS304L) sheet was investigated. The results show that lowering the temperature during deformation increases α'-martensite volume fraction (MVF) in the formed part. In addition, a reforming tool path, i.e., with reverse forming to higher wall angles, can be employed to increase the MVF to nearly 95% along the entire formed wall when the temperature is lowered. Secondly, numerical simulations were utilized to understand the plastic deformation under different loading histories during DSIF, which was related to the MVF observed in the experiments. This work demonstrates how IF can be utilized to tailor the final material properties of a formed part.

## 2. Experimental setup

DSIF experiments were performed on a fully austenitic stainless steel (SS304L) sheet of 1.5 mm thickness using the equipment shown in Fig. 1. A truncated square pyramid was formed with target dimensions of 90 mm base, 45° wall angle, and 30 mm flat top (Fig. 2). Two hemispherical-tip tools with 10 mm diameter made of A2 steel were utilized to form and support the sheet on each side during DSIF.

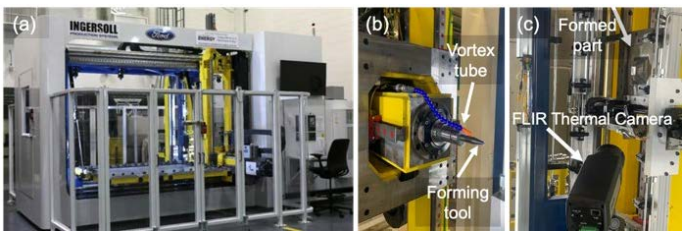


**Fig. 1** Experimental setup: (a) DSIF machine, (b) forming tool and vortex tube for cooling, and (c) FLIR camera for temperature measurement

To control the forming temperature, two vortex tubes located 40 mm away from the tool tips were used to blow air on each side of the sheet during DSIF (Fig. 1b). Note that the temperature increases during forming due to deformation-induced heating. A FLIR infrared (IR) thermal camera (SC-645; range of -20 to 650°C, resolution of 0.05°C, and spatial resolution of 640 x 480 pixels) was used to measure the temperature field as each pyramid was formed. The emissivity was calibrated for a lubricated surface and found to be 0.92 at 75 °C, which is the average temperature during the IF for the different cooling conditions in this research. The FLIR Research IR software was used to analyse the thermal images, which were captured at 1Hz. Fig. 1c shows the position of the camera in the setup.

For the DSIF experiments, three temperature conditions were used. Two utilized the vortex tubes at cold and ambient air temperatures and the other was without airflow, i.e., vortex tube air, compressed air, and no cooling cases, respectively. First, the vortex tubes with the inlet air pressure set at 690 kPa were adjusted to achieve a low temperature of -25°C at the nozzle, giving an air flow at the tool tip of -7.6°C, measured with a K-type thermocouple with an accuracy of ±1°C. Second, the vortex tubes were adjusted to blow compressed air at 18.2°C, which is the same temperature as the air entering the vortex tube system. The input pressure for this ambient temperature example was decreased to 255 kPa, so that these two airflow conditions were similar, i.e., 16.5 m/s with a mass flow rate of 590 $cm^3/s$, as measured with an anemometer.

In addition to temperature, the deformation path effect was examined by implementing a reforming concept with three steps. The square pyramid with a 90mm base, 30mm flat top, and 15° wall angle was first created in the negative z-direction. Then, in the second pass, the part was inverted to form the pyramid in the positive z-direction, creating a truncated pyramid with the same base and top but a 30° wall angle. Finally, the pyramid was formed in the third pass to the target 45° wall angle in the negative z-direction, which is the final target geometry (Fig. 3). This was compared with the pyramid formed to the 45° final wall angle geometry in a single pass. In this paper, a pass is defined as the process of the tool traveling over the workpiece and deforming it into the geometry defined by the programmed code for the DSIF machine.

A total of six experimental cases were run, twice in variable sequence to confirm repeatability, including two deformation paths (single pass and reforming) and three temperatures (vortex tube air, compressed air, and no cooling) conditions. A bidirectional z-level toolpath with a constant feed rate of 1500 mm/min and a step down of 0.3 mm was used to form the pyramids. The gap between the tools was calculated using the sine law, which estimates the thinning of the material as a function of the wall angle. The squeeze factor for the equation was 0.95. The third pass of reforming and the single pass cases used the same toolpath, and both took approximately 1300 s to complete. Motorcraft PTFE Lubricant XG-8 was sufficiently applied to both sides of the sheet before each forming pass to prevent wiping away by the tools. Thus, the emissivity value was assumed to be unchanged during forming.

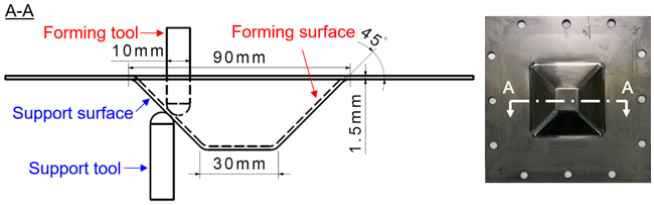


**Fig. 2** Target geometry and tooling/surface definitions

## 3. Numerical model

The effect of deformation path in the single pass and reforming cases was investigated using finite element (FE) simulations with ABAQUS/Explicit software. The blank was represented using 52640 linear brick elements with reduced integration (C3D8R) with a finer mesh in the center forming region of 0.8 x 0.8 x 0.5 $mm^3$ size (Fig. 4). Two rigid hemispherical tips of the tool were constructed on each side of the blank, and the same toolpaths as the experiment were used in both single pass and reforming simulations. Isotropic material properties were considered with $J_2$-plasticity and Hockett-Sherby hardening law, i.e., $\bar{\sigma} = 2238 - 1947 \cdot \exp(-1.12\bar{\varepsilon}^{0.93})$, where these parameters were identified using uniaxial tension stress-strain results in the rolling direction obtained at 20 °C and 0.001 $s^{-1}$ strain rate.

Coulomb friction model was assumed with a constant coefficient of 0.1 between the tool and contact surfaces. Wall clock times for the simulations, when computed on 32 CPU cores with 10,000 mass scaling, were 32 hours for a single pass and 62 hours for reforming. Moreover, an additional step using ABAQUS/Standard was implemented to capture springback after boundary conditions were removed.

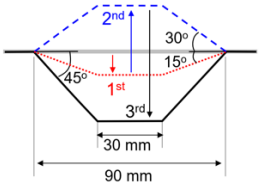


**Fig. 3** Three passes of reforming process

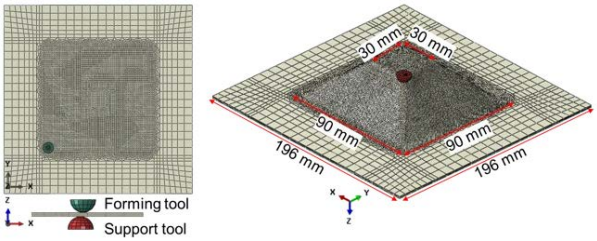


**Fig. 4** Schematic of FE simulation with blank mesh design

## 4. Experimental and numerical results

From the six experimental cases regarding forming temperature and deformation path, MVF change was compared at four evenly spaced points along the pyramid walls (Locations 1 – 4) using an FMP30C Feritscope (Fisher Technology Inc.), which is a non-destructive and easy method to measure MVF using the magnetic permeability of the material. Although this measurement method is known as less accurate than direct microstructure scanning, it gives reasonable results capturing the trend of MVF change [11].

The comparison results of MVF in the six DSIF forming conditions are summarized in Fig. 5. The line in this figure is the average MVF for the four walls, with each symbol (color designating the wall of the pyramid) being the average of ten Feritscope measurements per the specific wall location. The maximum standard deviation of a given measurement location was 4.3, which is approximately the size of the symbol. Fig. 6 compares the temperature for each experiment when the tool reaches Location 4. The effect of temperature is clearly seen in Fig. 5a: the MVF increases in order of vortex tube air, compressed air, and no cooling, as the temperature decreases (see Fig. 6), which is consistent with previous studies [9]. However, the no cooling condition shows the opposite trend of the highest MVF at Location 1 and lowest at Location 4. This is because the temperature of the sheet steadily rises throughout the deformation process in the

absence of augmented cooling (Fig. 7). The heat generated by large plastic deformation and friction between the tools and the sheet attenuates the martensite transformation kinetics.

In addition to lowering the temperature to increase MVF, inducing more deformation through the reforming produces a significant increase in the MVF value. In all three temperature cases, the MVF achieved in the reforming gradually increases as the number of passes increases (Fig. 5b) and is eventually more than doubled compared to the single pass case (Fig. 5a). This can be explained by comparing the deformation induced in the single pass and each pass of the reforming.

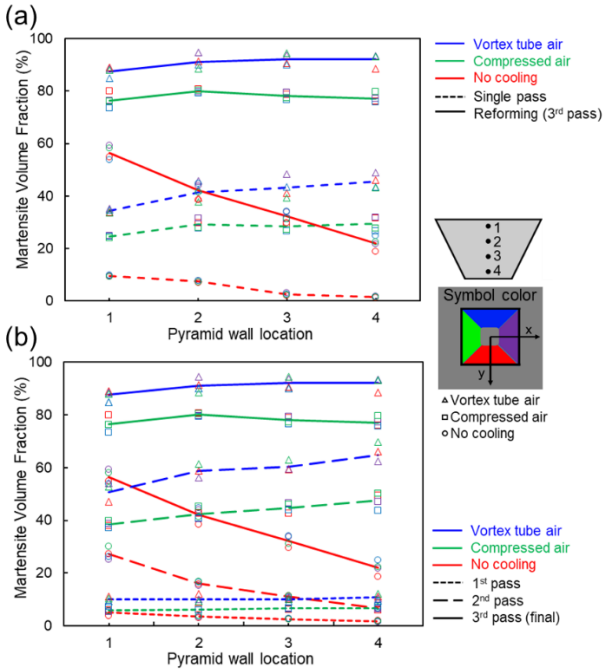


**Fig. 5** Martensite volume fraction change along the wall: comparison of (a) single pass and reforming and (b) number of passes in reforming

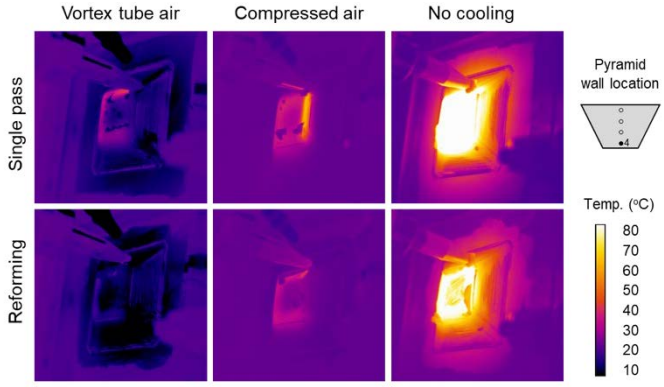


**Fig. 6** Temperature contours for each forming case at Location 4

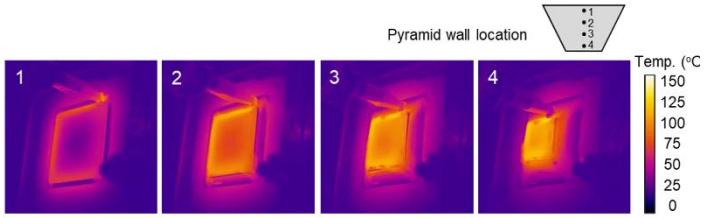


**Fig. 7** Single pass, no cooling case temperature contours (Locations 1–4)

As shown in Fig. 8, the equivalent plastic strain increases at each measurement location as the reforming process progresses from the 1st to the 2nd pass and from the 2nd to the final pass. This correlates to the increase of MVF in successive passes of reforming (Fig. 5b). In the same way, higher MVF of the final geometries for the reforming case can be explained by the higher equivalent plastic strain levels than the single pass case. It is worth noting that, the reforming, no cooling condition can produce similar MVF compared to the single pass, vortex tube air and compressed air cases (Fig. 5a). This indicates that the novel reforming strategy has more of an effect on the achievable MVF than decreasing the temperature.

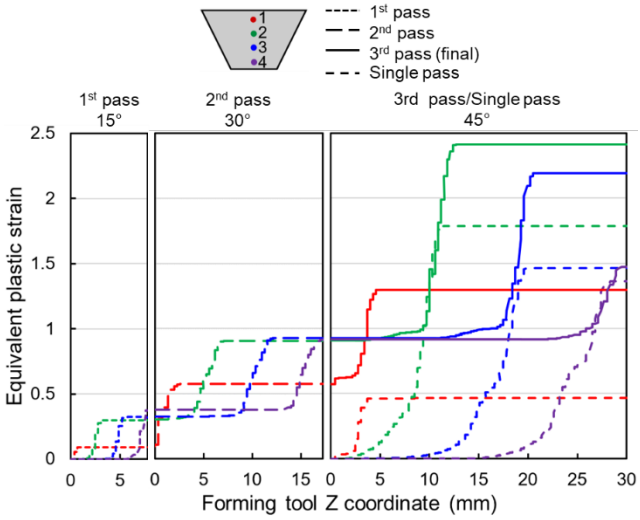


**Fig. 8** Equivalent plastic strain evolution along the wall for reforming passes and single pass case predicted by numerical simulations

In addition to the MVF, the cross-section profiles of the truncated pyramids were compared. Each specimen was unclamped after the pyramids were formed to the final geometry and scanned using a Faro Arm Quantumm laser line probe with an accuracy specification of ±0.025mm. Fig. 9 shows the profile comparison of the six DSIF experiments and the two simulations. It is seen that all experiments are close to the target geometry near the top of the pyramid (Location 4), but they start deviating near the flange area due to different springback effects.

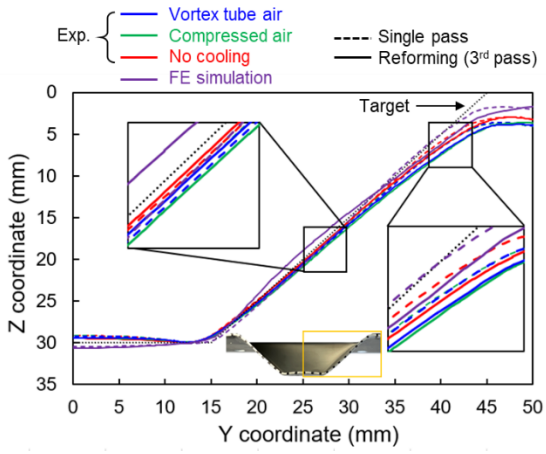


**Fig. 9** Profile comparison of six experiments and two simulations

As shown for the six experimental results in Fig. 9, both no cooling cases show less springback. This is influenced by the deformation induced heating (Figs. 6 and 7), which can lower the residual stresses that cause springback to occur. Also, comparing the reforming and single pass cases at the same cooling condition shows that the single pass case has a more accurate geometry. The

presence of residual stresses at the bending region near the base and the top of the truncated pyramid for the reforming case (Fig. 10) causes higher springback and inferior geometrical accuracy. Note that the vortex tube and compressed air cases are nearly identical with respect to the profile (Fig. 9) despite having ~10% differences in MVF.

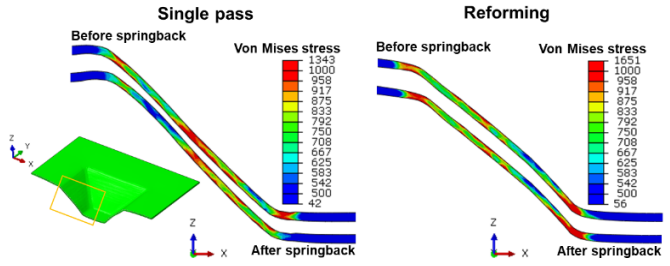


**Fig. 10** Effect of springback on von Mises stress contours through thickness in reforming and single pass cases

Furthermore, it is worth mentioning that the predicted profiles from the simulations are in good agreement with the experiments (Fig. 9); however, a deviation exists at the center of the inclined wall of the pyramid for the reforming case. The error in the prediction is caused by simplifications in the model, e.g., not considering the machine compliance, generated heat during deformation, material anisotropy, and martensite transformation. Another deviation exists at the bottom face of the pyramid, where the simulations show a higher z-value than the experiments. This is due to the dynamic effects from mass scaling in the simulations, which is also affected by the element size and has been observed in other studies. Nevertheless, the results show that it is possible to manipulate the final MVF of the part by controlling temperature and deformation path while maintaining nearly the same final part geometry.

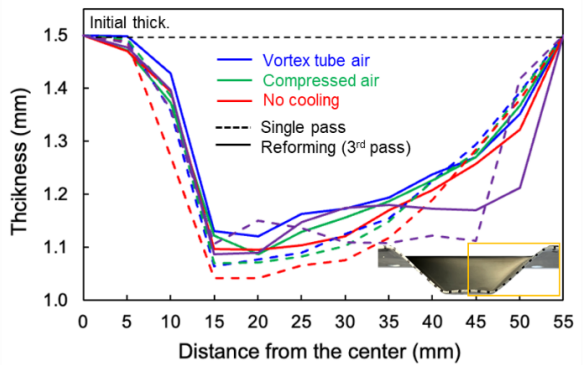


**Fig. 11** Thickness distribution of the experiment and simulation

After the profile scanning, parts were cut in half along the transverse to the rolling direction (y-direction). This made it possible to use a micrometer to measure the thickness along the cross-section profile of the specimens. Fig. 11 depicts the thickness distribution along the profile of the cross-section of the experiments, as well as the simulations. There are two main trends observed in the plot. First, the pyramids formed with the compressed air and vortex tubes are thicker than the ones formed with no cooling for the same final part geometry. This is due to the heat during deformation facilitating the elongation and thinning of the material. Second, the experiments with reforming show lower thinning due to the lower temperature rise, which inhibits thermal softening. This contradicts that the single pass led to better geometrical accuracy. The FE simulations predict a similar trend for the thickness distribution. The excessive thinning prediction near 45 mm from the center of the pyramid is caused by neglecting the tool deflection in the simulations.

## 5. Conclusions and outlook

Deformation path and temperature are two parameters that affect the MVF when forming austenitic stainless steels, e.g., SS304L. This paper showed that implementing a reforming process was able to increase the MVF in the formed part with or without cooling. If augmented cooling was implemented, the MVF obtained was increased. Part geometries were comparable despite the varying MVF values, although there was a slight variation in the thickness measurements. For the same part shape, the temperature and deformation path were able to generate MVF of less than 10% for the single pass, no cooling case, compared to 95% for the reforming, vortex tube air case. Additionally, using numerical simulations, strain histories and residual stresses were examined to explain the higher MVF and springback observed for reforming cases.

As for future work, to validate the MVF measurements in this study, electron backscatter or neutron diffraction could be used to compare with the Feritscope data. Although as mentioned previously, the Feritscope was shown in past research to provide reliable trends with respect to MVF measurements. Also, more accurate numerical models can be developed incorporating machine compliance, material anisotropy, and MVF evolution through a user defined material model. This would provide a further fundamentally understand of the factors that affect phase transformation and geometrical differences so that IF processes could be designed to create heterogeneous material properties for a given application.

## Acknowledgements

Funding for the NH BioMade Project from the U.S. National Science Foundation EPSCoR award (#1757371) is gratefully acknowledged.

## References

[1] Jeswiet, J., Micari, F., Hirt, G., Bramley, A., Duflou, J., & Allwood, J. (2005). Asymmetric single point incremental forming of sheet metal. CIRP annals, 54(2), 88-114.

[2] Duflou, J. R., Habraken, A. M., Cao, J., Malhotra, R., Bambach, M., Adams, D., Vanhove, H., Mohammadi, A., & Jeswiet, J. (2018). Single point incremental forming: state-of-the-art and prospects. International Journal of Material Forming, 11(6), 743-773.

[3] Moser, N., Ndip-Agbor, E., Ren, H. Q., Zhang, Z. X., Ehmann, K., & Cao, J. (2015). Challenges and process strategies concerning multi-pass double sided incremental forming. In Key Engineering Materials (Vol. 651, pp. 1122-1127). Trans Tech Publications Ltd.

[4] Wang, H., Zhang, R., Zhang, H., Hu, Q., & Chen, J. (2018). Novel strategies to reduce the springback for double-sided incremental forming. The International Journal of Advanced Manufacturing Technology, 96(1), 973-979.

[5] Peng, W., & Ou, H. (2023). Deformation mechanisms and fracture in tension under cyclic bending plus compression, single point and double-sided incremental sheet forming processes. International Journal of Machine Tools and Manufacture, 184, 103980.

[6] Ren, H., Xie, J., Liao, S., Leem, D., Ehmann, K., & Cao, J. (2019). In-situ springback compensation in incremental sheet forming. CIRP Annals, 68(1), 317-320.

[7] Moser, N., Leem, D., Ehmann, K., & Cao, J. (2021). A high-fidelity simulation of double-sided incremental forming: Improving the accuracy by incorporating the effects of machine compliance. Journal of Materials Processing Technology, 295, 117152.

[8] Feng, Z., Mamros, E. M., Ha, J., Kinsey, B. L., & Knezevic, M. (2021). Modeling of plasticity-induced martensitic transformation to achieve hierarchical, heterogeneous, and tailored microstructures in stainless steels. CIRP Journal of Manufacturing Science and Technology, 33, 389-397.

[9] Katajarinne, T., Louhenkilpi, S., & Kivivuori, S. (2014). A novel approach to control the properties of austenitic stainless steels in incremental forming. Materials Science and Engineering: A, 604, 23-26.

[10] Mamros, E. M., Maaß, F., Hahn, M., Tekkaya, A. E., Ha, J., & Kinsey, B. L. (2022, May). Superposing tensile stresses into single point incremental forming to affect martensitic transformation of SS304. In IOP Conference Series: Materials Science and Engineering (Vol. 1238, No. 1, p. 012085). IOP Publishing.

[11] Talonen, J., Aspegren, P., & Hänninen, H. (2004). Comparison of different methods for measuring strain induced α-martensite content in austenitic steels. Materials Science and Technology, 20(12), 1506-1512.